AIMS Materials Science, 12(3): 703–727.
DOI: 10.3934/matersci.2025030
Received: 13 May 2025
Revised: 15 July 2025
Accepted: 23 July 2025
Published: 29 July 2025

http://www.aimspress.com/journal/Materials

Research article

Flexural capacity of stainless-steel reinforced-concrete elements

Mokhtar Khalifa, Maged A. Youssef * and Mohamed Monir Ajjan Alhadid

Civil and Environmental Engineering, Western University, London, ON N6A 5B9, Canada

*** Correspondence:** Email: youssef@uwo.ca; Tel.: +1-519-661-2111 ext. 88661.

Abstract: Stainless steel (SS) is increasingly utilized in construction due to its robust strength and exceptional corrosion resistance. However, the lack of a defined yield point for SS introduces challenges in accurately calculating the moment of resistance for SS-reinforced concrete (RC) sections. To tackle this issue, a combined experimental-numerical study was conducted to pinpoint the stress in SS rebars that correlates with the moment of resistance of SS RC sections. This study tested four beams and four columns using two types of stainless steel: Austenitic (316 LN) and Duplex (2205). Following the experimental phase, a sectional analysis model was developed, validated through experimentation, and employed in a detailed parametric study. This research led to the creation of formulas that enable engineers to predict the moment of resistance for SS RC sections more precisely than current methods allow.

Keywords: concrete; stainless steel; reinforcement; yield; flexure; beams; experiment, analytical model

1. Introduction

The flexural design of reinforced concrete (RC) sections is typically performed based on the stress-block parameters [1]. This approach considers a fictitious rectangular stress block instead of the nonlinear stress distribution. The flexural capacity is estimated by satisfying the equilibrium conditions, assuming that the stress in the carbon steel rebars equals their yield stress. As this is not the case for stainless steel (SS), engineers usually estimate the yield stress using the 0.2% offset method. The accuracy of the resulting moment capacity for an SS RC section is unknown.

Austenitic SS has 17%–25 % chromium and 8%–26 % nickel [2]. It is widely available as a low-carbon chromium-nickel alloy (grades 304, 304L, 316, and 316L) containing up to 0.3% carbon [2].

It has excellent toughness, ductility, and weldability and is widely used in chloride environments. Duplex SS has a binary structure of ferrite and austenite [2]. It contains up to 8% nickel and between 22% and 28% chromium. It has improved strength and corrosion resistance compared to austenitic SS [3]. Duplex SS grades include 2205, 2304, and 2507.

Rabi et al. [4] performed an experimental-numerical study to examine the behavior of SS RC beams. The study proposed using the continuous strength method to predict the bending capacity of SS RC beams, a deformation-based design method. It enables accounting for material strain hardening properties and is thus suitable for SS material. Regardless, the technique diverges from traditional methods employed by engineers. Li et al. [5] conducted experimental tests on SS RC beams and validated the results using finite element analysis. Rabi et al. [6] stated that further studies are needed to understand the structural performance of SS RC whole systems. Zhang et al. [7] conducted hammer impact tests on RC bridge piers reinforced with stainless steel bars. Test results showed that using stainless steel for RC piers instead of carbon steel improved impact resistance, flexibility, and energy absorption capabilities.

Recent studies have explored the use of stainless steel in composite systems beyond its use as internal reinforcement. Lai et al. [8] investigated ultra-high-performance concrete (UHPC)-filled SS tubular columns under monotonic and cyclic loading, demonstrating increased transverse-to-longitudinal strain and enhanced ductility resulting from delayed confinement effects beyond peak load. Lai et al. [9] examined axially loaded SS tube-confined UHPC stub columns, reporting improved axial capacity and proposing design formulations to predict it. While these studies adopt deformation-based approaches for tubular systems, the present work focuses on SS as internal reinforcement. It introduces a closed-form stress substitution method compatible with RC code-based design. Together, these studies represent complementary advances in the structural application of stainless steel.

This paper investigates the flexural performance of SS RC members, including beams and axially loaded columns, through a multi-stage approach. It begins with tensile testing of austenitic and duplex SS bars to determine their mechanical properties. Subsequently, experimental tests are conducted on full-scale SS RC beams and columns. A sectional analysis model is then developed and validated against the experimental results. The validated model is used to perform a parametric study, from which simplified design equations are proposed to estimate the equivalent proof stress in stainless steel corresponding to the flexural capacity of SS RC sections.

2. Material characterization (tension tests)

In the first stage of the study, tensile tests were conducted on Austenitic and Duplex SS bars to define their constitutive relationships. These material models serve as input for the numerical simulation, facilitating accurate prediction of member-level behavior.

2.1. Methodology for the tension tests

Axial tensile tests were performed on Austenitic SS bars of sizes 15, 20, and 30 mm and 15 and 20 mm Duplex SS bars. Three specimens of each size were tested. The tensile tests were conducted per ASTM A370 [10] and ASTM A276 [11]. Each specimen was subjected to a monotonic tensile load in a displacement-controlled manner at a rate of 0.1 mm/min until the tangential modulus began to decrease, then the strain rate was increased to 2.2 mm/min until failure. The displacement was

measured automatically by the movement of the machine head. In contrast, the strains at the central part of each bar were measured using a linear electrical resistance strain gauge. The test setup and a close-up view of the strain gauge are shown in Figure 1a,b, respectively.

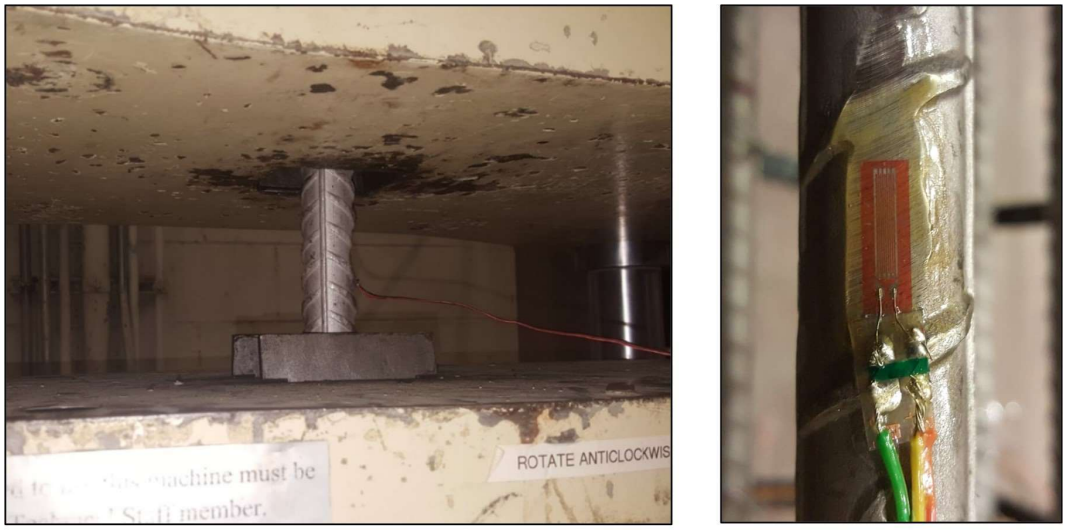

Figure 1. Tensile test of stainless-steel bars. (a) SS bar during testing and (b) attached strain gauge.

2.2. Results of the tension tests

Figure 2a,b show the average recorded stress-strain curves for Austenitic and Duplex SS bars, respectively. Considering all the conducted tests, the maximum deviation in results for one bar size was about 3% for duplex SS bars and about 5% for austenitic SS bars. The bar diameter and the SS type affected the stress-strain curves. Failure of all specimens was governed by necking, followed by a fracture within the gauge length away from the machine grips. All bars showed a ductile failure mode, as indicated by the significant deformation before fracture.

Duplex bars exhibited higher uniform elongation and a steeper strain-hardening slope, with ultimate stress exceeding the 0.2% proof stress by approximately 30%–35%, compared to more modest hardening in austenitic bars.

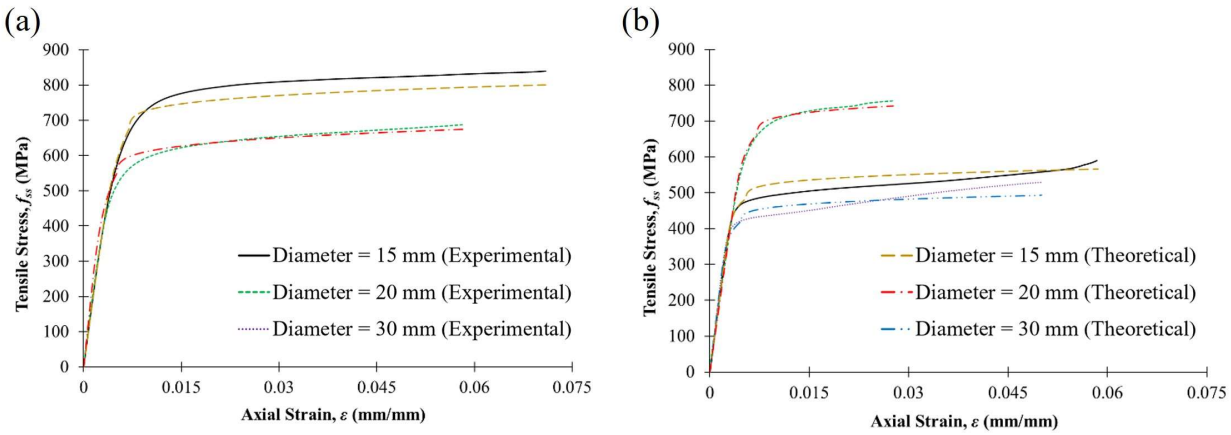

Figure 2. Stress-strain curves of the experimentally tested SS bars. (a) Duplex 2205 and (b) Austenitic 316 LN.

2.3. Discussion of the tension tests

The theoretical stress-strain curve by Ramberg-Osgood [12] (Eq 1) and Rasmussen [13] (Eq 2) is used to idealize the obtained experimental curves. The input parameters were obtained from the experimental results and are summarized in Table 1. The theoretical curves based on these parameters are shown in Figure 2a,b.

$$\varepsilon = \frac{\sigma}{E_o} + 0.002\left(\frac{\sigma}{\sigma_{0.2}}\right)^n, for\ \sigma \le \sigma_{0.2} \quad (1)$$

$$\varepsilon = \frac{\sigma-\sigma_{0.2}}{E_o} \times \left(1 + 0.002 \times \frac{n \times E_o}{\sigma_{0.2}}\right) + \left(1 - \frac{\sigma_{0.2}}{\sigma_u}\right) \times \left(\frac{\sigma-\sigma_{0.2}}{\sigma_u-\sigma_{0.2}}\right)^m + \frac{\sigma_{0.2}}{E_o} + 0.002, for\ \sigma > \sigma_{0.2} \quad (2)$$

Where σ and ε are the stress and strain values, and factors n and m determine the sharpness of the stress-strain curve and can be calculated as follows: $n = \frac{\ln(20)}{\ln(\sigma_{0.2}/\sigma_{0.01})}$ and $m = 1 + 3.5\frac{\sigma_{0.2}}{\sigma_u}$; stresses $\sigma_{0.01}$, $\sigma_{0.2}$, and σ_u are the 0.01% proof stress, 0.2% proof stress, and ultimate stress, and E_o is the initial modulus of elasticity.

Table 1. Mechanical properties of stainless steel bars, including E_o measured from the linear portion (≤ 0.01% strain) of the experimental stress-strain curve.

No.	Bar diameter (mm)	Bar type	$\sigma_{0.01}$ (MPa)	$\sigma_{0.2}$ (MPa)	E_o (MPa)	σ_u (MPa)
1	15	Duplex	426	675	136,363	845
2	20	Duplex	331	550	178,125	746
3	15	Austenitic	400	483	141,500	600
4	20	Austenitic	525	663	130,434	800
5	30	Austenitic	330	420	156,875	530

3. Experimental program

Following the tensile tests conducted on SS bars, an experimental program was undertaken to evaluate the load-deformation behavior and failure mode of SS RC beams and columns. The outcomes are used to validate the sectional analysis model described in Section 4.

3.1. Beams (flexure)

The flexural behavior of the four SS RC beams listed in Table 2 was evaluated experimentally. Each beam measured 250 mm in width, 400 mm in overall depth, and 2440 mm in length, with a clear span of 2200 mm. Closed carbon steel stirrups (Table 2) were spaced to ensure that the factored shear resistance exceeded 1.5 times the factored shear demand, thereby suppressing diagonal cracking and enforcing flexural failure. Shear checks were performed using Eq 11.4 of CSA A23.3-14, with resistance factors set to unity for test-level evaluation.

A 35 mm clear concrete cover was adopted to accommodate strain gauge instrumentation on the soffit bars while maintaining adequate bond. This value aligns with the Class F1 exposure category in Table 17 of CSA A23.3, which permits a minimum cover of 30 mm for cast-in-place concrete in dry interior environments and 40 mm in more aggressive conditions; 35 mm represents a conservative intermediate value consistent with common detailing practices.

Carbon steel was used for the top reinforcement because the beams were simply supported and the top bars remained in compression. This choice facilitated the anchorage of the closed stirrups and reduced material cost without affecting the tensile performance of the stainless steel, which was the focus of the study. SS bars were used only in the bottom layer to isolate their flexural contribution and to ensure a clear soffit for instrumentation. This arrangement also reduced the risk of galvanic corrosion, as it avoided direct contact between dissimilar alloys in exposed zones. All stirrups were fabricated from carbon steel in accordance with standard practice, since corrosion-resistant transverse reinforcement is typically not required when cover is adequate.

Table 2. Description of the beam specimens.

Specimen designation	Type of bottom steel bars	Bottom steel bars	Top steel bars (carbon steel)	Stirrups (carbon steel)[1]
B1	Duplex SS	3M20	2M10	M10@200 mm
B2	Austenitic SS	3M30		
B3	Duplex SS	5M20		
B4	Austenitic SS	5M30		

[1]Note: Stirrup spacing satisfies CSA A23.3-14.

The mechanical properties of concrete are determined by testing seven standard concrete cylinders per ASTM C39 [14]. The average 28-day concrete compressive strength and modulus of rupture were found to be 37.0 and 3.1 MPa, respectively. Figure 3 shows the steel cages for the four beams. Four strain gauges were mounted on each beam's top and bottom longitudinal rebars at the mid-span section. The concrete was cured by covering it with moist burlap.

Figure 3. Steel cages of the tested beams.

3.1.1. Beam test setup

The four beams were tested in a one-point loading scheme, as shown in Figure 4. This loading setup was selected to create a well-defined peak moment region at mid-span, simplify the test configuration, and allow precise instrumentation at the point of maximum curvature to observe flexural behavior and localized failure modes. The load-deflection curve and deformation behavior were obtained using linear variable displacement transducers (LVDTs), which were installed at the soffit of the beams at their mid-span section. The load was applied using a load-controlled hydraulic actuator at a rate of 20 kN/s. Testing was terminated when concrete crushing was observed at the extreme compression fiber.

Figure 4. Beam test setup.

3.1.2. Beam test results

The load-deflection curves at the mid-span section for the tested beams are shown in Figure 5. Technical issues prevented recording deformations for B1. The deformation behavior of the beams shows a similar trend to the stress-strain curves of the embedded SS bars, which lack a well-defined

yield plateau. The larger failure deflections observed in duplex-reinforced beam B3 are attributed not only to stress distribution but also to enhanced ductility and pronounced strain hardening of the duplex bars. The higher uniform elongation capacity allows greater post-yield strain, enabling larger curvature before failure. Furthermore, the rising tensile force due to strain hardening delays the onset of concrete crushing, thereby extending the deflection trajectory. Figure 5 shows that increasing the reinforcement ratio does not significantly affect the deformation behavior. However, it has a significant influence on both stiffness and ultimate capacity. The average stiffness of B4 is 25% higher than that of B2. The flexural capacity of B4 is 18.5% higher than that of B2, and that of B3 is 37% higher than that of B1. The crack patterns are depicted in Figure 6. A photo of beam B2 at the end of the test is shown in Figure 7.

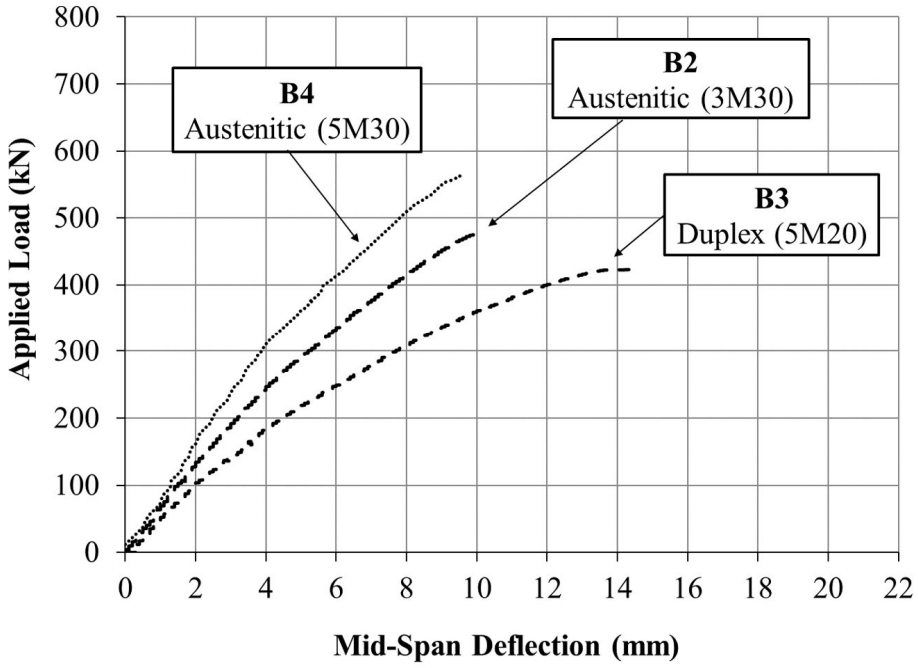

Figure 5. Mid-span load-deflection curves for beams B2, B3, and B4. (B1 omitted—LVDT record incomplete).

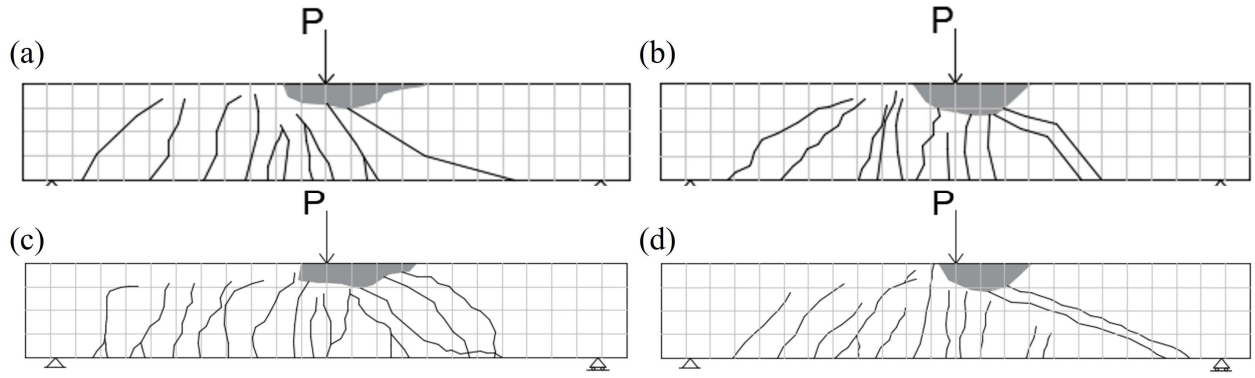

Figure 6. Crack patterns of the tested beams at failure. (a) Beam B1, (b) Beam B2, (c) Beam B3, and (d) Beam B4.

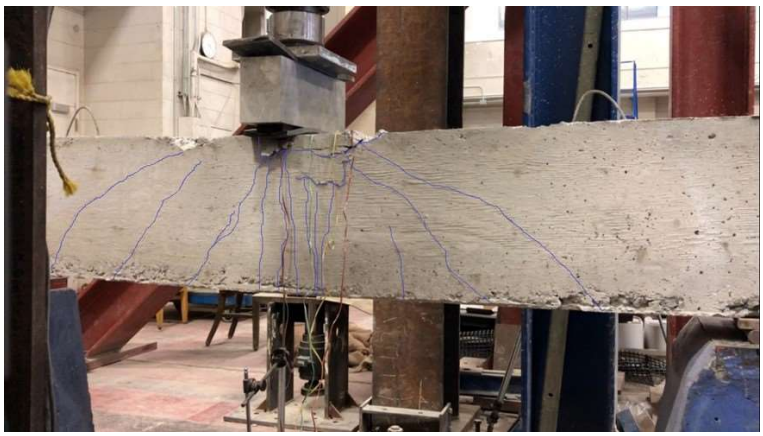

Figure 7. Crack pattern for B2 at failure.

The variation of strains with load at the mid-span section was recorded at the top and bottom reinforcing bars. All strain gauges installed at the same level for each beam showed almost identical readings. The strain profiles at the mid-span section of the tested beams at failure are depicted in Figure 8. Generally, the flexural capacity of the tested beams was reached when the strain at the extreme compression fiber was within the range of 0.0030–0.0035. The corresponding strains of Duplex and Austenitic SS bars showed differences with values of 0.0103, 0.00344, 0.0062, and 0.0026 for B1, B2, B3, and B4, respectively. The higher strain values for Duplex SS RC sections explain the higher ultimate deflection in Beam B3 compared to Beams B2 and B4. This behavior is also attributed to the enhanced ductility and pronounced strain hardening of duplex SS bars, which allow greater deformation capacity beyond initial yielding.

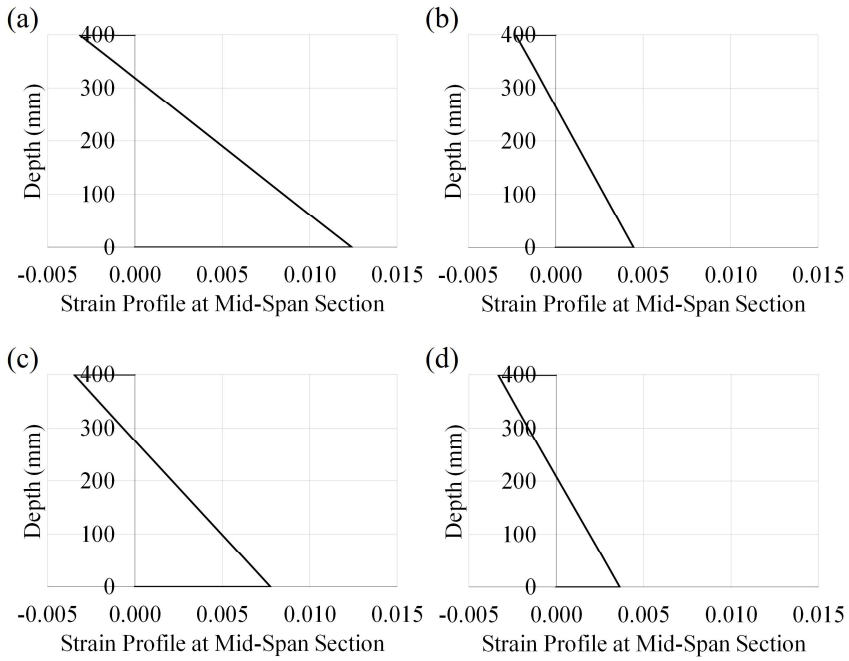

Figure 8. Strain profile at mid-span section of the tested beams at failure. (a) Beam B1, (b) Beam B2, (c) Beam B3, and (d) Beam B4.

3.2. Columns (eccentric compression)

Four stainless-steel RC columns were tested, as shown in Table 3. The examined columns have cross-sectional dimensions of 300 mm by 300 mm and a total height of 2200 mm. Tie spacing (Table 3) satisfied confinement requirements and provided shear resistance exceeding 1.6 times the calculated demand, ensuring flexural-compression failure rather than shear failure.

Table 3. Column specimens.

Specimen designation	Type of longitudinal steel bars	Longitudinal steel bars	Column ties(carbon steel)[1]
C1	Austenitic	12M20	10M@180 mm
C2	Duplex		
C3	Austenitic	10M15	
C4	Duplex		

[1]Note: Tie spacing meets CSA A23.3-14 Clause 10.7 [1] confinement criteria.

3.2.1. Column test setup

Two cantilevers are constructed at the ends of each column to facilitate the application of an eccentric axial load at one end and provide stable support at the other. Both cantilevers had a depth of 700 mm and a width of 300 mm. The erected steel cages are shown in Figure 9. Four strain gauges are attached to the longitudinal bars at the mid-height of each column. The concrete columns are constructed from the same concrete mix used in the beams. Monotonic load with an eccentricity of 400 mm was applied through a load-controlled hydraulic actuator at a 20 kN/s loading rate, as illustrated in Figure 10. Lateral deflection at the mid-height of each column was obtained using an LVDT.

Figure 9. Steel cages of the tested columns.

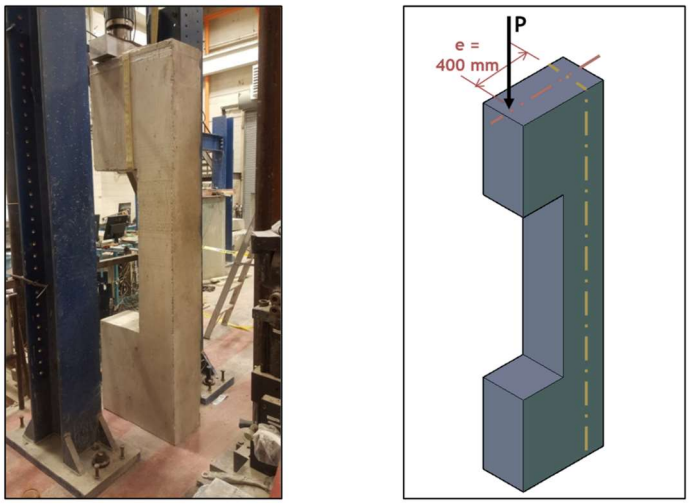

Figure 10. Test setup for the SS columns. (a) Column sample and (b) schematic view.

3.2.2. Column test results

The mid-height lateral load-deflection responses of columns C1, C2, and C4 are shown in Figure 11. Increasing the longitudinal reinforcement ratio led to a corresponding increase in peak axial load capacity: 11.5% (C1 vs. C3) and 34.0% (C2 vs. C4). A representative photograph of column C1 after testing is provided in Figure 12, and Figure 13 shows the observed cracking patterns at failure for all four specimens. All columns exhibited similar deformation behavior. Flexural tension cracks initiated at the front face of the column near the top cantilever, followed by compression crushing on the opposite interior face. This failure localization occurred in the upper third of the prismatic column body, just below the cantilever–column interface.

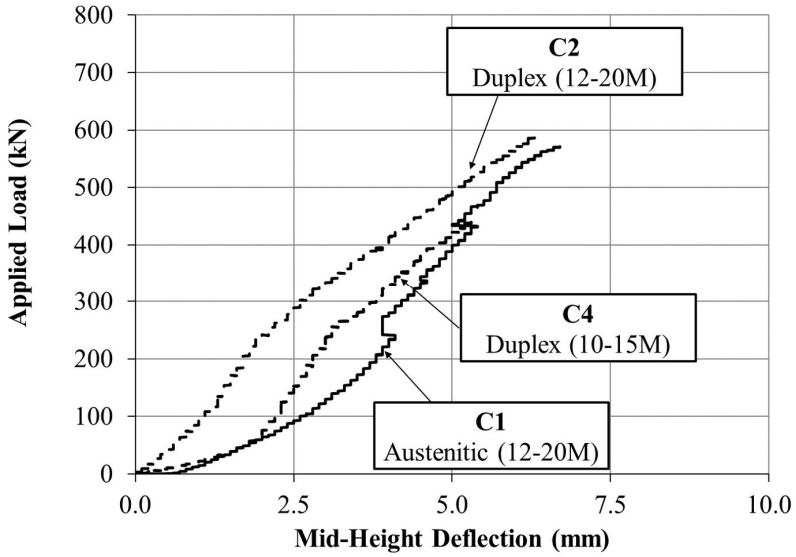

Figure 11. Mid-height lateral-deflection curves for columns C1, C2, and C4. (C3 omitted—LVDT dropout at ≈ 40% P_{max}).

Although curvature along the column height should theoretically be symmetric under uniform section properties and end eccentricities, the cantilever was seated on the lab floor, distributing the reaction over a broad area. In contrast, the applied load at the top was concentrated through a bearing plate. This asymmetry induced a non-uniform curvature distribution and shifted the peak moment region upward, thereby concentrating damage near the upper load introduction zone. The cantilever stubs remained largely elastic and served solely as load transfer fixtures.

Figure 12. Failure mode of column C1.

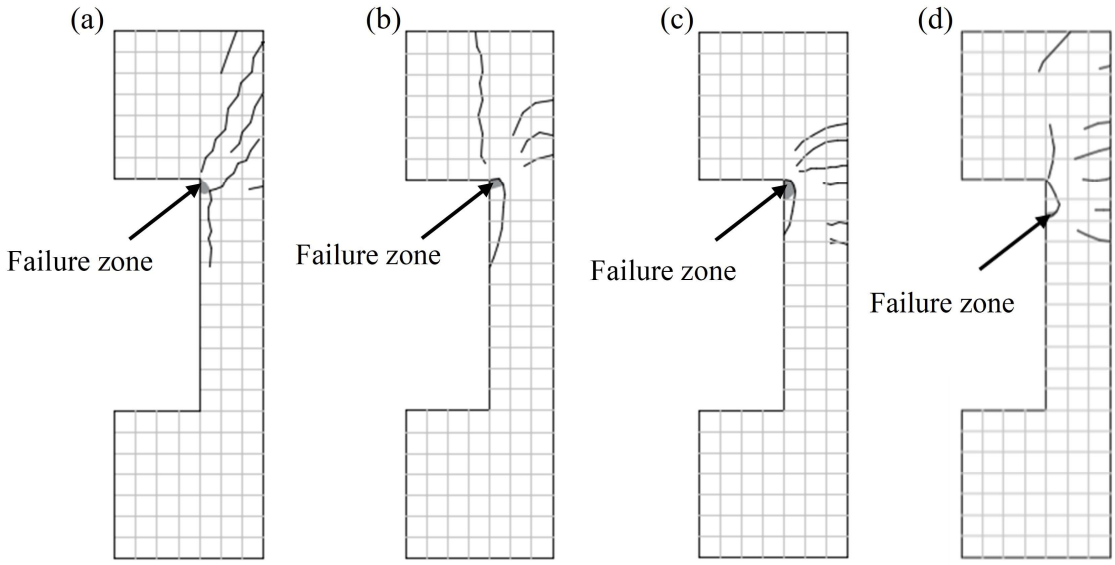

Figure 13. Cracking pattern of the tested columns at failure. (a) Column C1, (b) Column C2, (c) Column C3, and (d) Column C4.

Strain variation is measured and recorded by installing strain gauges on the longitudinal bars at the mid-height of the examined columns. Two strain gauges, one on each side, are attached to the opposite bars to verify the measurements and to detect any out-of-plane deformation. The strain gauges on the same side of each column showed consistent readings without significant variation in the values. The recorded strain values at the interior and exterior reinforcing bars plot the strain profiles at mid-height of columns C1 through C4 at failure, as shown in Figure 14.

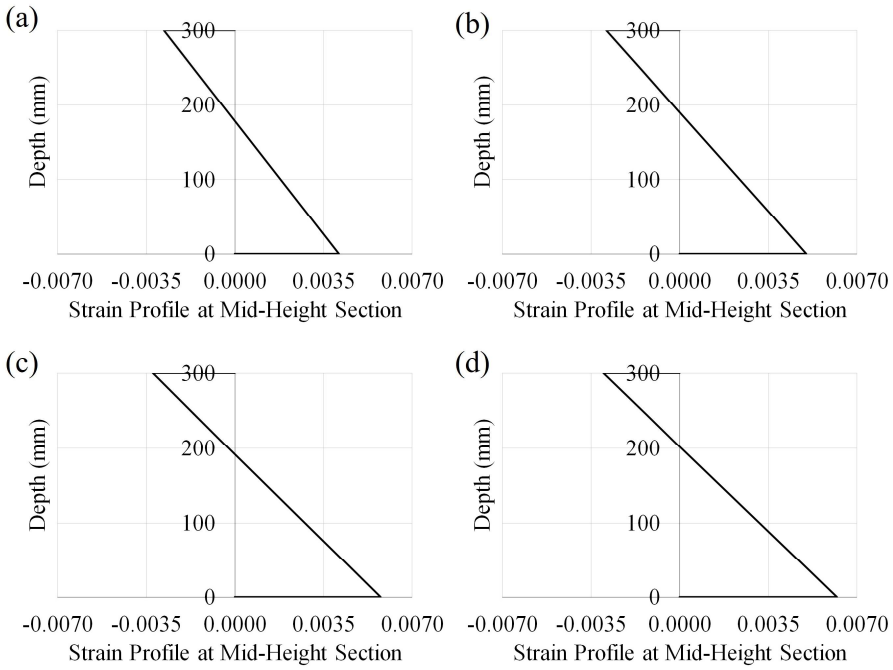

Figure 14. Strain profile at mid-height section of the tested columns. (a) Column C1, (b) Column C2, (c) Column C3, and (d) Column C4.

The strain profiles show that failure of the tested columns occurred once the extreme compression fiber at the mid-height section reached a strain value between 0.0029 and 0.0033. Varying the SS bar type was found to have a minor influence on the strain profiles. The load-strain curves at mid-height of column C4 are shown in Figure 15. Compressive strains were detected at all loading values for the inner reinforcing bars until the concrete crushed, at which point the strain in the compression bars reached 0.0013. This value corresponds to a strain in the extreme compression fiber of 0.0031.

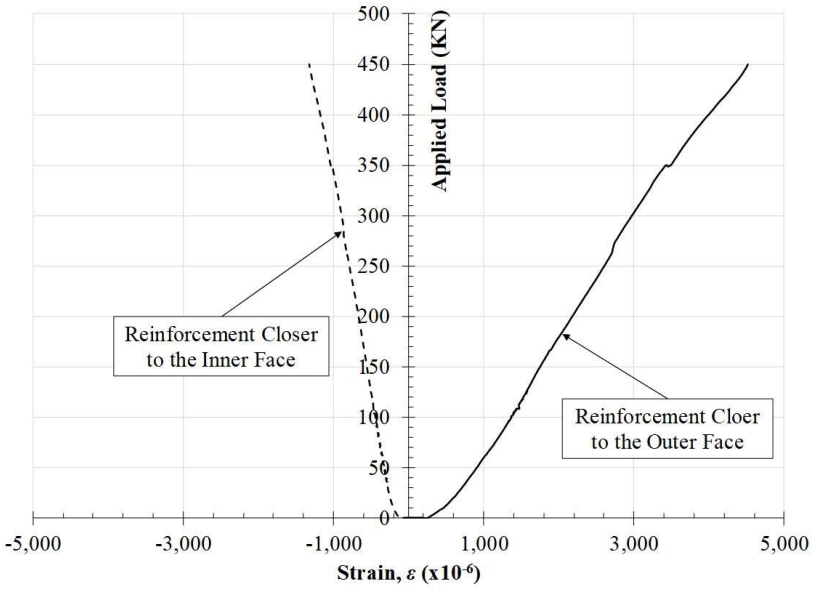

Figure 15. Variation of strain in the bars at the mid-height section.

4. Sectional analysis model

Following the experimental program, a sectional analysis model (Figure 16) [15–17] was developed to predict the flexural strength and deformation behavior of SS-RC members. Once validated, the model enables the parametric study in Section 4.4, from which simplified design guidance is derived.

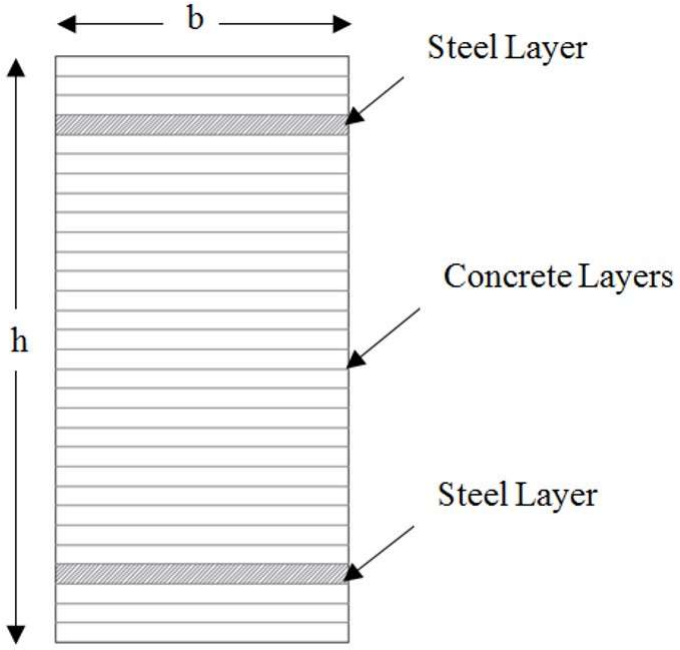

Figure 16. Typical mesh for the sectional analysis method.

4.1. Formulation and implementation

The mechanical properties were based on compression tests performed on concrete cylinders and tensile tests performed on SS bars. The numerical model was implemented and executed using MATLAB [18]. The numerical simulation was conducted using a custom-developed MATLAB code. The code was specifically written to model the behavior of SS RC members, taking into account the material's nonlinear stress-strain relationship and the governing equations for flexural capacity. Assumptions for the numerical model include the following: plane sections remain plane, a perfect bond exists between concrete and the embedded SS bars, geometrical nonlinearity is not considered, sufficient reinforcement is provided to prevent shear failure, and failure happens when the extreme compression fiber reaches a strain value of 0.0035 as defined by CSA A23.3 [1]. The constitutive relationship proposed by Scott et al. [19] was adopted in the numerical model to describe the behavior of concrete in compression. Concrete was assumed to have negligible tensile strength at all loading stages. Constitutive relationships for the SS bars followed the model proposed by Rasmussen [13]. The analysis was performed by applying incremental curvature and calculating the strain at each layer based on its location relative to the centroid. The applied curvature was gradually increased until the concrete reached the crushing strain at its extreme compression fiber. The moment-area method was then used to determine the load-deflection curve at the mid-span section based on a one-point loading scheme.

4.2. Model validation against beam tests

The capability of the proposed model to predict strength and deformation behavior was validated, given the experimental results. A comparison between the experimental and numerical load-deflection curves for the tested beams is shown in Figure 17. The sectional analysis approach accurately predicted the flexural capacity of the SS-RC elements. The calculated percentage differences for the flexural capacity are 1.7%, 3.4%, 5.2%, and 6.3% for beams B1 through B4. The higher hardening slope used for duplex bars in the numerical model reflects their measured strain-hardening behavior, allowing the model to reproduce the increased curvature capacity observed experimentally.

4.3. Model validation against column tests

The proposed model was validated against experimental results for columns C1, C2, and C4 under eccentric loading. Figure 18 compares the experimental and numerical load-deflection curves, demonstrating strong agreement. The predicted flexural capacities differed from test values by 5.5%, 4.7%, and 1.1%, respectively. These results confirm the model's ability to capture the axial–flexural interaction and the influence of reinforcement and axial load level on column behavior.

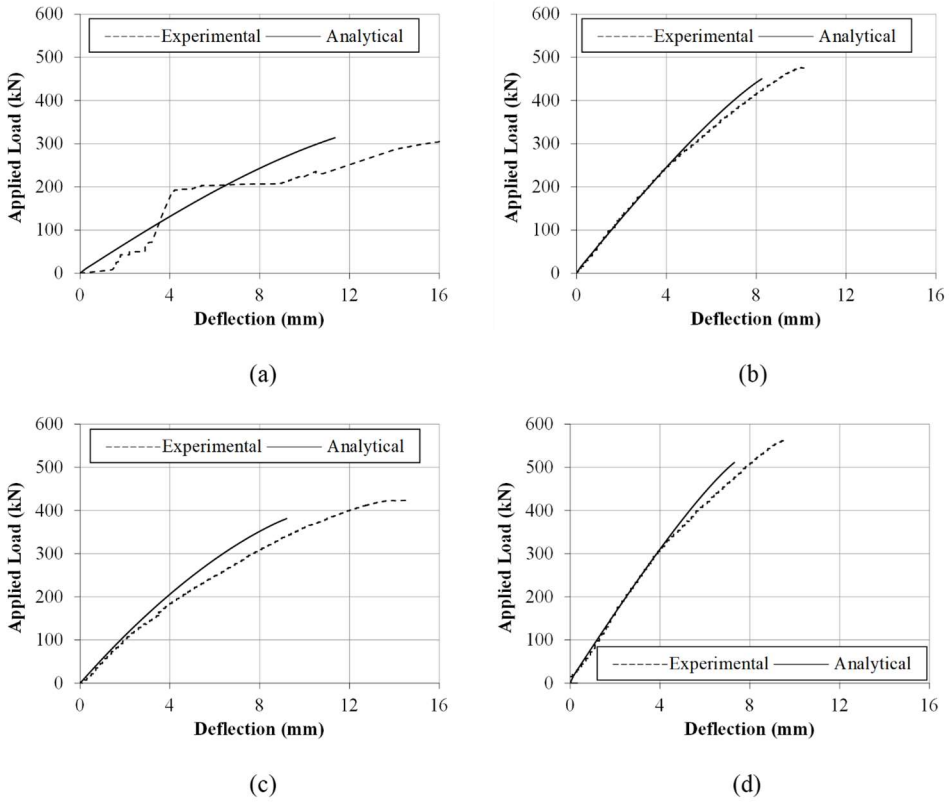

Figure 17. Validation of the numerical model considering the beam tests. (a) Beam B1, (b) Beam B2, (c) Beam B3, and (d) Beam B4.

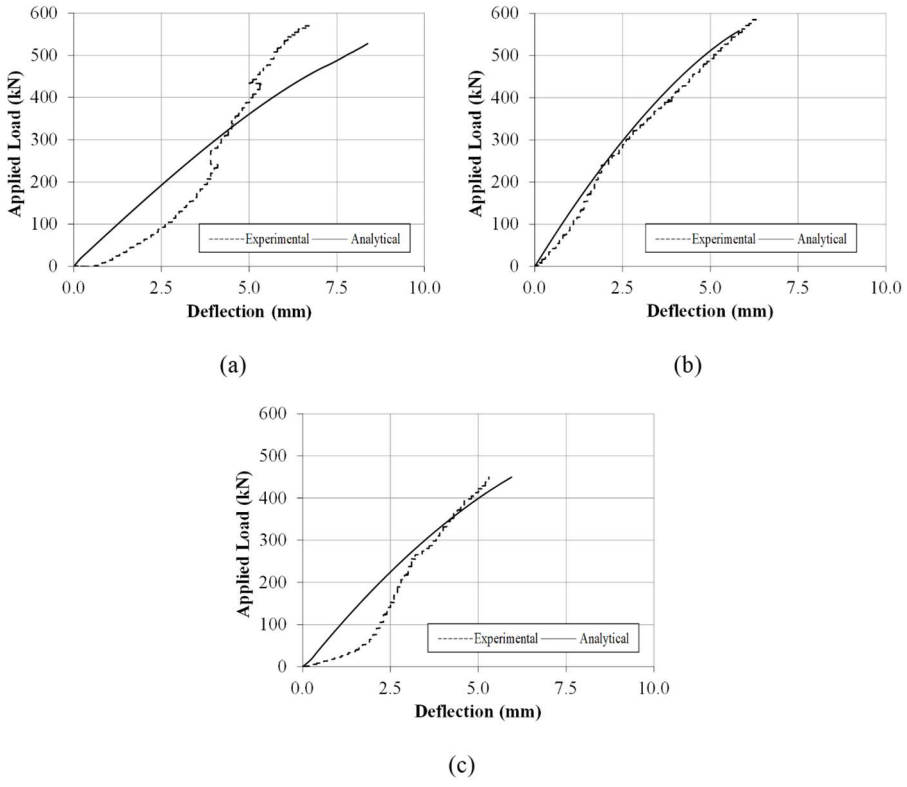

Figure 18. Validation of the numerical model considering the column tests. (a) Column C1, (b) Column C2, and (c) Column C4.

4.4. Parametric study

Following the validation of the numerical model in Sections 4.2 and 4.3, a parametric study was conducted to extend its application and systematically quantify the stress developed in SS bars under ultimate conditions. The outcomes form the basis for the practical design expressions presented in Section 5.

The cross-sectional dimensions and reinforcement ratios are summarized in Tables 4 and 5. The parameters considered are SS type (Austenitic or Duplex), cross-sectional dimensions (width b and height h of 300, 650, and 1000 mm), reinforcement ratios ρ for the beams (minimum, average, and maximum values as per the Canadian Highway Bridge Design Code [20]), ρ for the columns (2.0%, 3.0%, and 4.0%), axial load level, $\left(\lambda = \frac{Applied\ Load}{Column\ Capacity}\right)$, for the columns (0.1 and 0.2).

Table 4. Dimensions and reinforcement ratios of the beam parametric study.

Specimen No.	Other parameters	Reinforcement ratio	b (mm)	h (mm)
B1	Austenitic or Duplex	0.0023	300	300
B2		0.0019		650
B3		0.0018		1000
B4		0.0022	650	300
B5		0.0019		650
B6		0.0017		1000
B7		0.0022	1000	300
B8		0.0019		650
B9		0.0017		1000
B10		0.0187	300	300
B11		0.0182		650
B12		0.0178		1000
B13		0.0186	650	300
B14		0.0182		650
B15		0.0178		1000
B16		0.0186	1000	300
B17		0.0182		650
B18		0.0178		1000
B19		0.0350	300	300
B20		0.0345		650
B21		0.0338		1000
B22		0.0350	650	300
B23		0.0345		650
B24		0.0338		1000
B25		0.0350	1000	300
B26		0.0345		650
B27		0.0338		1000

Table 5. Dimensions and reinforcement ratios of the column parametric study.

Specimen No.	Other parameters	Reinforcement ratio	b (mm)	h (mm)
C1	Austenitic or Duplex	0.02	300	300
C2	λ = 0.1 or 0.2			650
C3				1000
C4			650	300
C5				650
C6				1000
C7			1000	300
C8				650
C9				1000
C10		0.03	300	300
C11				650
C12				1000
C13			650	300
C14				650
C15				1000
C16			1000	300
C17				650
C18				1000
C19		0.04	300	300
C20				650
C21				1000
C22			650	300
C23				650
C24				1000
C25			1000	300
C26				650
C27				1000

Figures 19–22 show the influence of the considered parameters on the SS stress (f_{ss}) at failure. For the beams, section dimensions were found to have a negligible impact on f_{ss}. Although increasing the section dimensions increases the moment capacity, the associated increase in the steel area results in a similar strain distribution at the peak moment. The width had a negligible influence on columns. However, increasing the section height for columns resulted in an initial increase in f_{ss}. This increase is linked to the axial load and the compression steel. Changing the number of steel bars was found to have a significant impact on the stresses developed in the SS bars for beams and columns. In general, increasing the reinforcement ratio results in reducing f_{ss} since the ultimate capacity is reached at a smaller curvature.

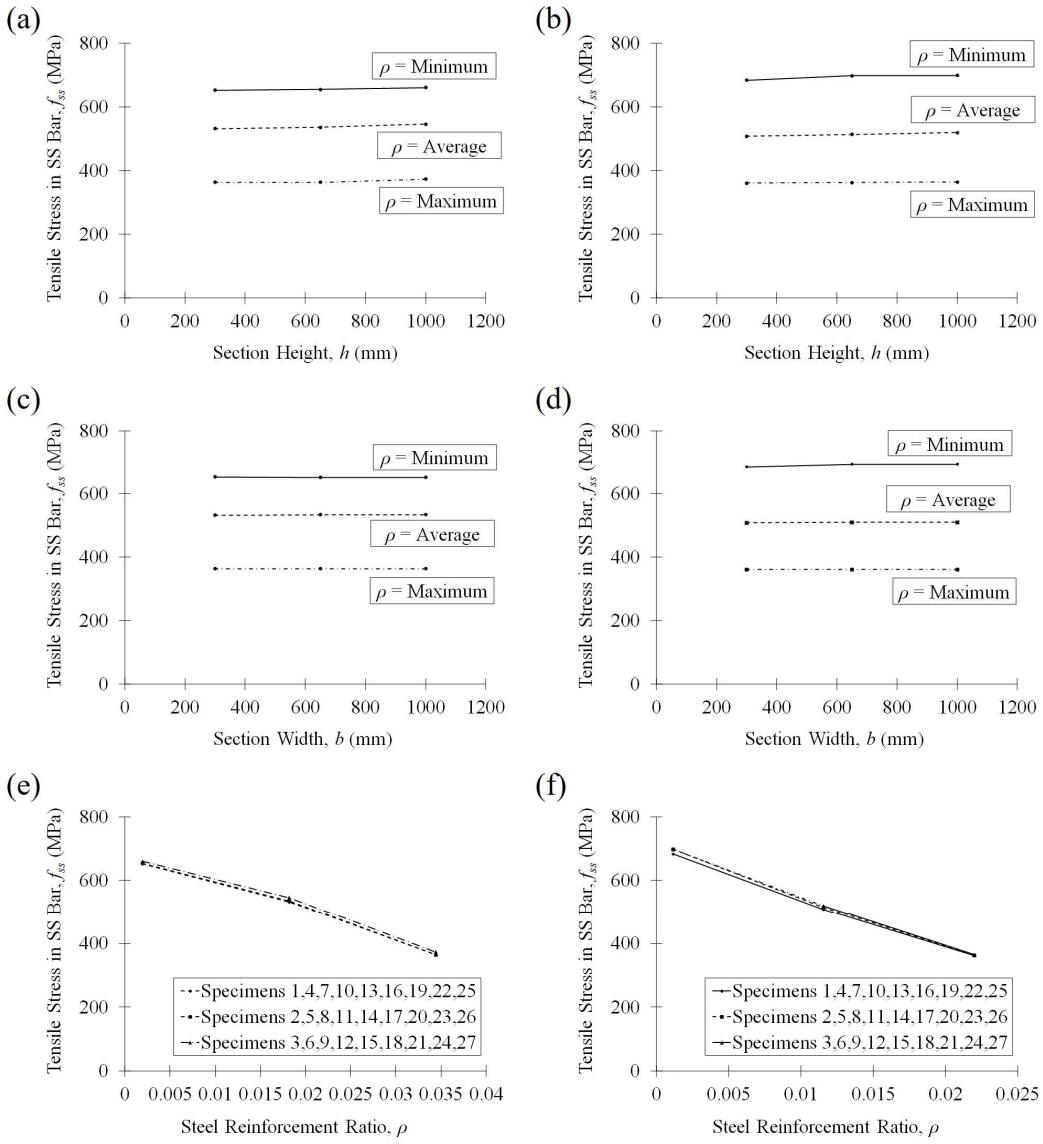

Figure 19. Tensile stress in the SS bars at M_R for the beam specimens. (a) Section height (Austenitic), (b) section height (Duplex), (c) section width (Austenitic), (d) section width (Duplex), (e) steel reinforcement ratio (Austenitic), and (f) steel reinforcement ratio (Duplex).

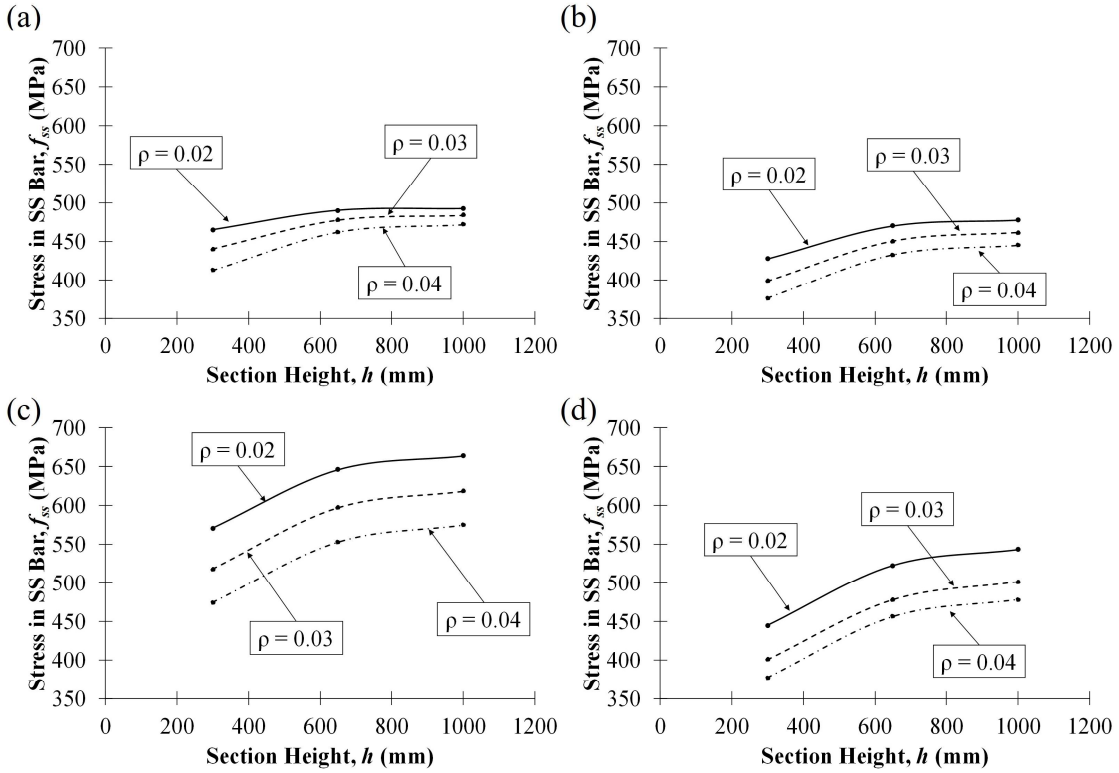

Figure 20. Influence of varying h on fss in stainless-steel RC columns. (a) Austenitic (λ = 0.1), (b) Austenitic (λ = 0.2), (c) Duplex (λ = 0.1), and (d) Duplex (λ = 0.2).

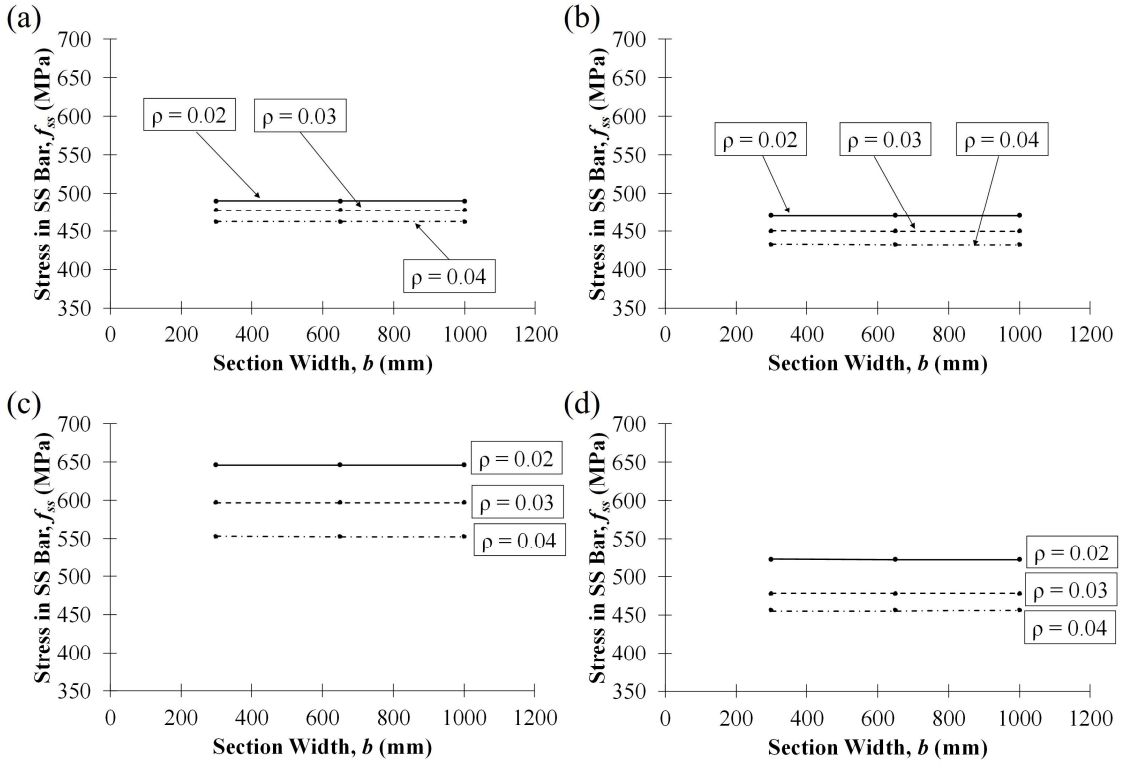

Figure 21. Influence of varying b on fss in stainless-steel RC columns. (a) Austenitic (λ = 0.1), (b) Austenitic (λ = 0.2), (c) Duplex (λ = 0.1), and (d) Duplex (λ = 0.2).

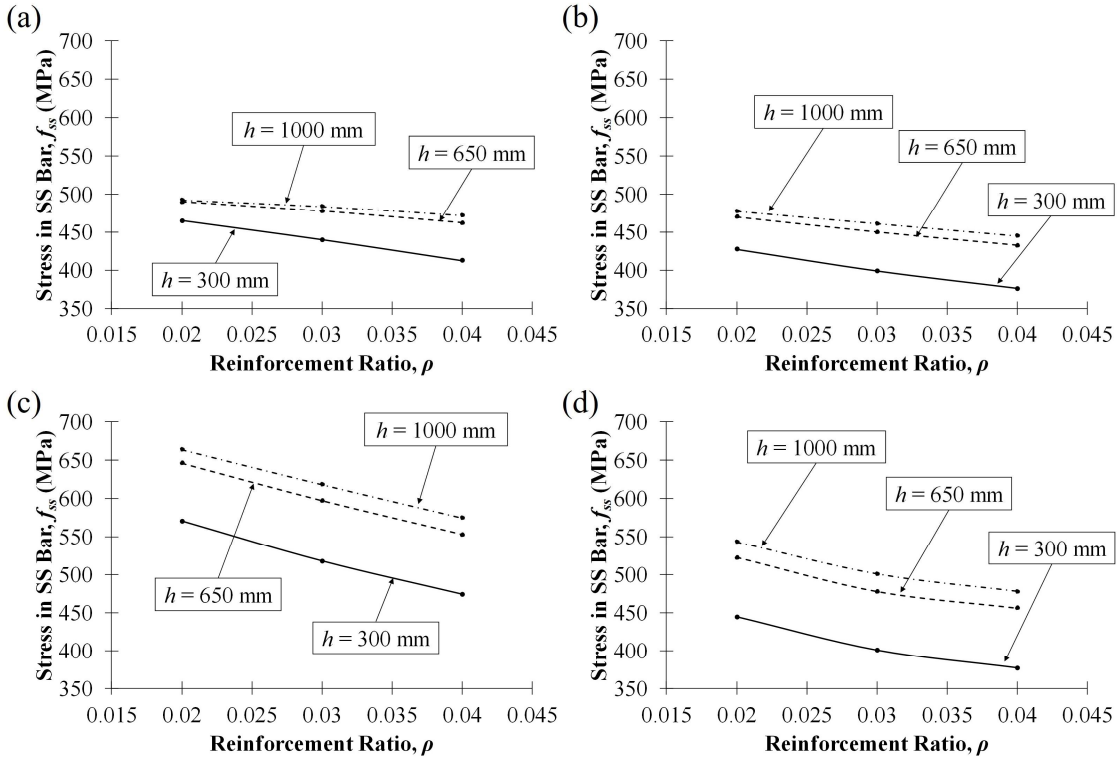

Figure 22. Influence of varying ρ on *fss* in stainless-steel RC columns. (a) Austenitic (λ = 0.1), (b) Austenitic (λ = 0.2), (c) Duplex (λ = 0.1), and (d) Duplex (λ = 0.2).

5. Design equations and working example

Based on the validated parametric study presented in Section 4.4, the influence of key parameters, such as reinforcement ratio, section height, and axial load level, on the equivalent reinforcement stress was quantified. This section translates those findings into practical design expressions.

Applying the CSA A23.3 [1] procedure to calculate the flexural capacity of SS RC members requires knowledge of the yield stress of the reinforcing bars. Since SS bars lack a well-defined yield plateau, an equivalent stress must be evaluated to establish the equilibrium condition. This study proposes a method based on the validated parametric study to determine the f_{ss} of Duplex and Austenitic SS bars.

Regression analysis was implemented to determine the best-fit equation that describes the relationship between the equivalent stress and the investigated parameters. The value of the equivalent yield stress was found to be highly correlated with ρ. For beams, the influence of the section's cross-sectional dimensions and concrete mechanical properties was found to be negligible. Based on that, Eqs 3 and 4 are proposed to calculate f_{ss} for Austenitic and Duplex SS bars, respectively. Similarly, regression analysis is used to determine expressions for calculating the equivalent stress in columns. Eqs 5 and 6 are proposed to calculate f_{ss} for Austenitic and Duplex stainless-steel bars, respectively.

$$f_{ss} = -102063\rho^2 - 5196\rho + 666.59 \geq 360 \text{ MPa, for Beams \& Austenitic 316LN} \quad (3)$$

$$f_{ss} = 56611\rho^2 - 12308\rho + 719.11 \geq 360 \text{ MPa, for Beams \& Duplex 2205} \quad (4)$$

$$f_{ss} = 500.0 - 568.9\rho - 95.9\lambda - 0.0093h, \text{for Columns \& Austenitic 316LN} \quad (5)$$

$$f_{ss} = 704.4 - 1067.8\rho - 580\lambda + 0.082h, \text{for Columns \& Duplex 2205} \quad (6)$$

The calculation procedure for the flexural capacity of the SS RC members relies on the λ acting on the members. If $\lambda = 0$, the member is considered a beam element. Eqs 3 and 4 calculate an equivalent yield stress, which will be substituted into the equilibrium equation according to CSA A23.3 [1]. However, if $0 < \lambda \leq 0.2$, then Eqs 5 and 6 are used to calculate the stresses in the SS bars. Then, the equilibrium condition is established, and the corresponding flexural capacity is calculated. A complete working example for a representative beam is provided in the Appendix to demonstrate the full calculation process.

The proposed simplified procedure was validated against the experimental results of the tested beam and column specimens. The proposed method exhibits excellent prediction potential considering the actual behavior of the stainless-steel bars, as illustrated in Figures 23 and 24. A comparison between the proposed equation and the experimental results revealed an excellent agreement, as indicated by average errors of 3.9% and 5.7% for the beam and column specimens, respectively. The negligible presence of outliers results in higher confidence in the proposed procedure.

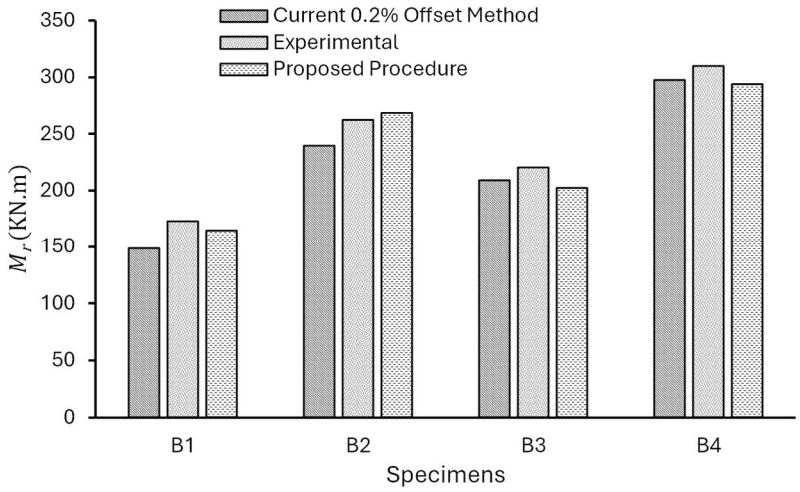

Figure 23. Accuracy of predicting M_R for experimentally tested beams.

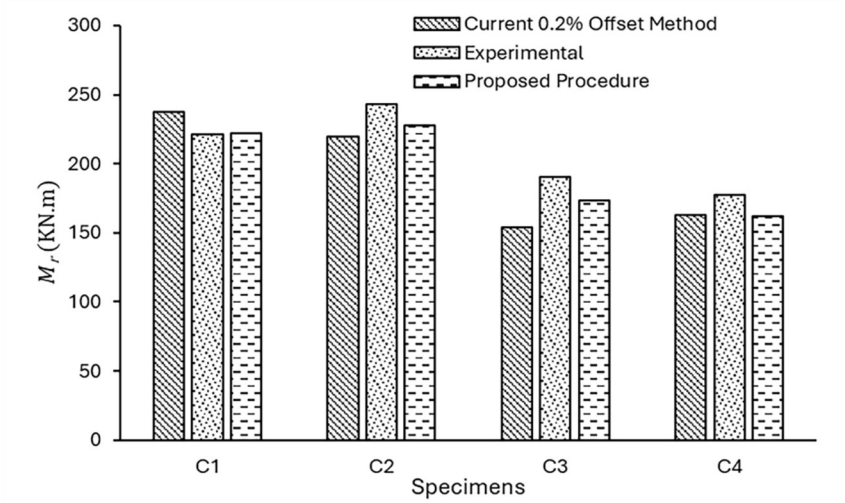

Figure 24. Accuracy of predicting M_R for experimentally tested columns.

The proposed procedure was also validated against the numerical results obtained from the parametric study in Figure 25. The equality plot line for all specimens reveals that the proposed procedure provides a better approximation of the moment of resistance of SS RC sections than the current 0.2% offset method. The proposed equation revealed an average error of 3.7% and 4.8% for beams and columns, respectively, while the current 0.2% offset method indicated an average error of 24.3% and 14.1% for beams and columns, respectively.

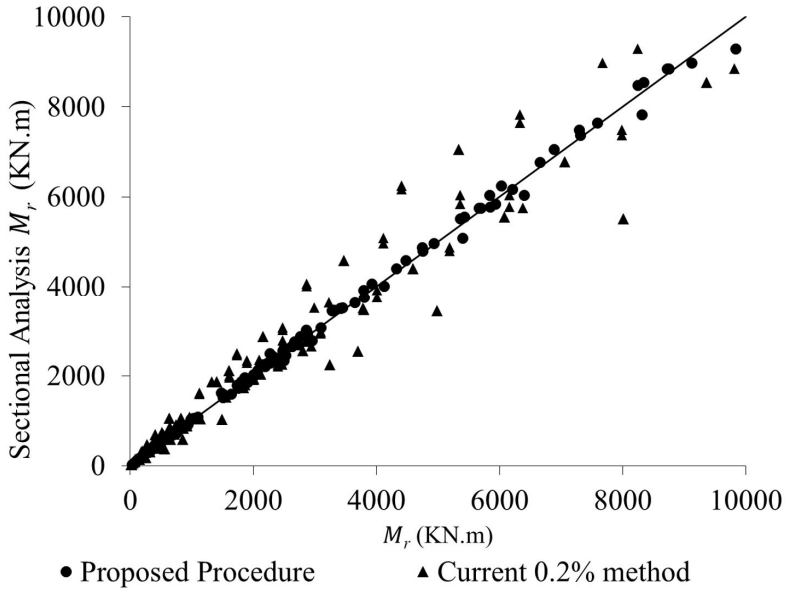

Figure 25. Accuracy of M_R for parametric study sections.

Compared to deformation-based approaches such as the continuous strength method (CSM), which require iterative sectional analysis using full nonlinear material models, the proposed equivalent-stress substitution method (ESSM) provides a closed-form solution that integrates directly with standard code-based flexural design checks. It requires only readily available parameters such as bar yield strength and reinforcement ratio for beams and, additionally, section height and axial load level for columns, with no need for strain calculations or iterative procedures. This ESSM enables compatibility with existing design workflows while maintaining high accuracy. The average error relative to full sectional analysis was 3.7% for beams and 4.8% for columns, which is significantly lower than the error associated with the traditional 0.2%-offset method. ESSM thus offers a practical and reliable tool for everyday design applications involving stainless steel reinforcement.

6. Conclusions

This paper describes the experimental and numerical programs conducted to evaluate the behavior of SS-RC members and proposes a procedure for calculating their flexural capacity. The study commenced by performing tensile tests on both Austenitic and Duplex SS bars to determine their mechanical properties and actual constitutive relationships. After that, four large-scale SS RC beams were tested in a one-point loading scheme to assess their flexural performance. Additional tests were conducted on four eccentrically loaded large-scale columns to investigate their deformation behavior and failure mode. A numerical model was then proposed and validated based on the experimental

results. The validated model was used to perform a parametric study investigating the influence of varying the cross-sectional dimensions, reinforcement ratio, SS type, and axial load level on the f_{ss} developed in the bars at failure. Fifty-four cases for beams and 108 cases for columns were examined. The results revealed that reinforcement ratio and axial load level are the main factors affecting the value of f_{ss}. The influence of section height becomes more pronounced as the axial load level increases. Finally, a regression analysis was performed, and mathematical expressions for the f_{ss} were proposed, which can be used to calculate the flexural capacity of SS RC members. While the proposed method utilizes separate expressions for beams and columns to maintain accuracy, future research is encouraged to develop a unified predictive model incorporating broader parametric coverage, including higher ρ values and intermediate axial load levels.

Use of AI tools declaration

The authors declare they have not used Artificial Intelligence (AI) tools in the creation of this article.

Acknowledgements

This research was funded by the Ministry of Transportation, Ontario (MTO). Salit Specialty Rebar donated the SS bars utilized in the experimental phase of the study.

Author contributions

Conceptualization: M.A.Y.; methodology: M.A.Y.; validation: M.K.; formal analysis: M.K.; investigation: M.K.; data curation: M.K.; writing—original draft preparation: M.K.; writing—review and editing: M.A.Y. and M.M.A.A.; visualization: M.K.; supervision: M.A.Y. and M.M.A.A.; project administration: M.A.Y.; funding acquisition: M.A.Y. All authors have read and agreed to the published version of the manuscript.

Conflict of interest

Maged A. Youssef is on a special issue editorial board for *AIMS Materials Science* and was not involved in the editorial review or the decision to publish this article. All authors declare that there are no competing interests.

References

1. CSA Group (2014) *Design of Concrete Structures (A23.3-14)*, 6th Eds, Ottawa, ON, Canada: CSA Group.
2. Nürnberger U (2005) Stainless steel reinforcement—A survey. *Otto Graf J* 16: 111–138.
3. Davis JR (1994) *ASM Specialty Handbook: Stainless Steels*, Ohio, USA: ASM International.
4. Rabi M, Cashell KA, Shamass R (2019) Flexural analysis and design of stainless steel reinforced concrete beams. *Eng Struct* 198: 109432. https://doi.org/10.1016/j.engstruct.2019.109432

5. Li Q, Guo W, Liu C, et al. (2020) Experimental and theoretical studies on flexural performance of stainless steel reinforced concrete beams. *Adv Civ Eng* 2020: 4048750. https://doi.org/10.1155/2020/4048750
6. Rabi M, Shamass R, Cashell KA (2022) Structural performance of stainless steel reinforced concrete members: A review. *Constr Build Mater* 325: 126673. https://doi.org/10.1016/j.conbuildmat.2022.126673
7. Zhang G, Xu S, Xie H, et al. (2017) Behavior of stainless steel–reinforced concrete piers under lateral impact loading. *Adv Mech Eng* 9: 168781401770993. https://doi.org/10.1177/1687814017709936
8. Lai BL, Li YR, Jin L, et al. (2024) Experimental study on the compressive behavior of UHPC filled stainless steel tubes subjected to monotonic and cyclic loading. *Constr Build Mater* 449: 138301. https://doi.org/10.1016/j.conbuildmat.2024.138301
9. Lai BL, Li YR, Becque J, et al. (2025) Axial compressive behavior of circular stainless steel tube confined UHPC stub columns under monotonic and cyclic loading. *Thin-Walled Struct* 208: 112830. https://doi.org/10.1016/j.tws.2024.112830
10. ASTM International (2014) Standard test methods and definitions for mechanical testing of steel products. ASTM A370, West Conshohocken, PA, USA.
11 ASTM International (2017) Standard specification for stainless steel bars and shapes. ASTM A276, West Conshohocken, PA, USA.
12. Ramberg W, Osgood W (1943) *Description of Stress-Strain Curves by Three Parameters. Technical Note No. 902*, Washington, DC, USA: National Advisory Committee for Aeronautics.
13. Rasmussen KJR (2003) Full range stress-strain curves for stainless steel alloys. *J Constr Steel Res* 59: 47–61. https://doi.org/10.1016/S0143-974X(02)00018-4
14. ASTM International (2003) Standard test method for compressive strength of cylindrical concrete specimens. ASTM C39, West Conshohocken, PA, USA.
15. Youssef MA, Rahman M (2007) Simplified seismic modeling of reinforced concrete flexural members. *Mag Concr Res* 59: 639–649. https://doi.org/10.1680/macr.2007.59.9.639
16. Alhadid MA, Youssef MA (2017) Analysis of reinforced concrete beams strengthened using concrete jackets. *Eng Struct* 132: 172–187. https://doi.org/10.1016/j.engstruct.2016.11.014
17. Alhadid MA, Youssef MA (2018) Assessment of the flexural behavior of reinforced concrete beams strengthened with concrete jackets. *Eng Struct* 167: 108–120. https://doi.org/10.1016/j.engstruct.2018.04.026
18. MATLAB (2019) *MATLAB R2019b User's Guide*, Natick, MA, USA: The MathWorks Inc.
19. Scott BD, Park R, Priestley MJN (1982) Stress-strain behavior of concrete confined by overlapping hoops at low and high strain rates. *ACI Struct J* 79: 13–27. https://doi.org/10.14359/10875
20. CSA Group (2014) *Canadian Highway Bridge Design Code (CSA S6-14)*, 11th Eds, Ottawa, ON, Canada: CSA Group.

Appendix

This example illustrates the calculation of flexural capacity for a stainless-steel-reinforced concrete (SS-RC) beam using the proposed equivalent stress method.

Given concrete properties:

- Section height, h = 400 mm
- Section width, b = 250 mm
- Concrete compressive strength, f_c' = 35 MPa
- Area of stainless steel reinforcement, A_s = 2100 mm^2
- Clear concrete cover, c = 35 mm
- Stirrup diameter, Φ = 10 mm
- Bar diameter, d = 30 mm

Step-by-step calculation:

1. Effective depth (d):

$$depth = h - c - \Phi - 0.5d = 400 - 35 - 10 - 0.5 \times 30 = 340\ mm$$

2. Reinforcement ratio (ρ):

$$\rho = \frac{A_s}{bd} = \frac{2100}{250 \times 340} = 0.0247$$

3. Equivalent reinforcement stress (f_{ss}):

Using Eq 3:

$$f_{ss} = -102063\rho^2 - 5196\rho + 666.59 = -102063(0.0247)^2 - 5196(0.0247) + 666.59 = 475.9\ MPa$$

4. Tensile force in the reinforcement (T_S):

$$T_s = f_{ss} \times A_S = 475.9 \times 2100 = 999.4\ kN$$

5. Equivalent concrete stress block parameters ($\alpha_1$and β_1)-clause 10.1.7 of A23.3:

$$\alpha_1 = 0.85 - 0.0015f_c' = 0.85 - 0.0015 \times 35 = 0.7975$$

$$\beta_1 = 0.97 - 0.0025f_c' = 0.97 - 0.0025 \times 35 = 0.8825$$

6. Neutral axis depth (C):

$$C = \frac{T_s}{\alpha_1 \times \beta_1 \times b \times f_c'} = \frac{999.4 \times 1000}{0.7975 \times 0.8825 \times 250 \times 35} = 162.3\ mm$$

7. Nominal moment capacity (M_r)

$$M_r = T_s\left(d - \frac{\beta_1 \times C}{2}\right) = 999.4 \times 1000 \times \left(340 - \frac{0.8825 \times 162.3}{2}\right) = 268.2\ kN.m.$$

AIMS Press

© 2025 the Author(s), licensee AIMS Press. This is an open access article distributed under the terms of the Creative Commons Attribution License (http://creativecommons.org/licenses/by/4.0)